Use of Standard CMOS Pixel Imagers as Ionizing Radiation Detectors

L. Servoli, D. Biagetti, D. Passeri and E. Spanti Gattuso

***Abstract*–The recent developments in the domain of the standard CMOS imagers for visible light, mainly in the reduction of the pixel size, has led us to investigate the suitability of some of these devices as ionizing radiation detectors. A standard 640x480 imager with 5.6x5.6 micrometer pixel size (Micron product type MT9V011) has been characterized with both photons (^{55}Fe and 8 keV X-ray tube) than charged particles sources (500 MeV electrons). The main results obtained are: a small pixel multiplicity (4-5), for the detection of either X-ray or charged particles; a good linearity of the response; a S/N ratio > 30 for a Minimum Ionizing Particle and an estimated sensitivity down to about 2 keV.**

I. Introduction

IN recent years, CMOS pixel imagers applications have grown at a phenomenal rate. Consumers are demanding more functionality, including advanced and robust imaging capabilities on DSCs and camera phones, as well as a growing emphasis on the number of pixels present on the same surface (several Megapixels devices are now normally available). Nowaday, a pixel size of less than 2 micrometers is available. Beside imaging applications, new perspectives in several research areas could be opened by such a class of devices. As an example, position measuring devices for ionizing radiation with submicrometer accuracy could be possible.

In this work, we have investigated the possibility of using MICRON (now Aptina Imaging) CMOS imagers as ionizing radiation detectors, either for X-ray than for charged particles. Different samples of a standard sensor featuring 640x480 pixel matrix, with 5.6x5.6 micrometers pixel size and 4.0 micrometers epitaxial layer depth [2] have been tested. The integration at sensors level of these features has been possible thanks to the progress of the microelectronics

These devices have a built-in 10-bit ADC conversion capability and also the possibility to adjust the gain of the circuit from 1.0 up to 15.88 [ref.]. The readout of the sensor is assured (fig. 1) by the *Demo2* board and the *MT9SH06* evaluation board, with an USB line to power the system, to control the sensor and to receive the data.

Manuscript received November 14, 2008. L. Servoli is with the Istituto Nazionale di Fisica Nucleare, Sezione di Perugia, Perugia, I-06132 Italy (telephone: +39-075-585-2706, e-mail: leonello.servoli@pg.infn.it).

D. Biagetti, is with Istituto Nazionale di Fisica Nucleare, Sezione di Perugia and Dipartimento di Ingegneria Informatica ed Elettronica, Universita' degli Studi di Perugia, Perugia, I-06132 Italy. (telephone: +39-075-585-2700, e-mail: daniele.biagetti@pg.infn.it).

D. Passeri, is with Istituto Nazionale di Fisica Nucleare, Sezione di Perugia and Dipartimento di Ingegneria Informatica ed Elettronica, Universita' degli Studi di Perugia, Perugia, I-06132 Italy. (telephone: +39-075-585-3643, e-mail: daniele.passeri@diei.unipg.it).

E. Spanti Gattuso is with Micron Technology Italia, Avezzano, L'Aquila, I-06132 Italy.

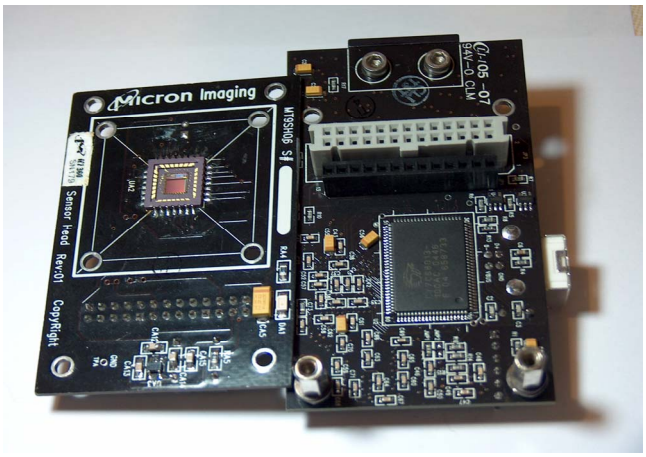

Fig. 1. MICRON MT9V011 evaluation board with a sensor embedded (left) and Demo2 readout board (right).

The sensors under test have no microlenses over the pixels and are run in monochromatic mode in order to extract the signal without the software corrections needed to compensate the pixel response to visible photons with different wavelenghts.

II. Electrical Characterization

The response of the sensor in absence of ionizing radiation sources has been studied; for each pixel the signal has been collected and the distribution is well represented by a gaussian fit.

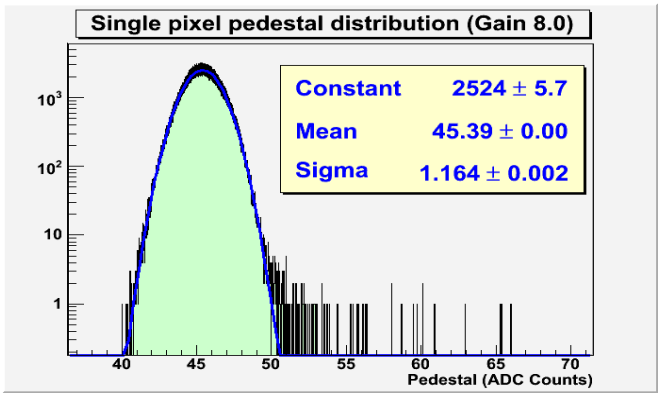

Fig. 2. Distribution of single pixel pedestal with superimposed a gaussian

The average signal and its RMS have been extracted from each fit and have been used as the pedestal and the noise of the

pixel. In fig. 2 it is reported the distribution of all the pedestals of a sensor and the shape is gaussian to a good approximation with a small standard deviation.

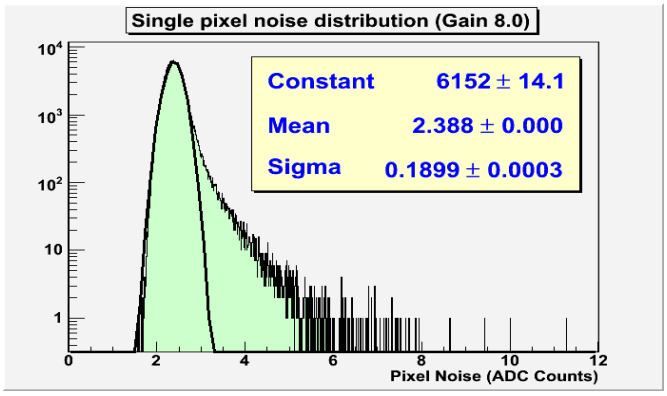

Fig. 3. Distribution of single pixel noise with superimposed a gaussian fit.

This is a good indication of the homogeneity of the sensor. Another indicator of the goodness of the sensor is (fig. 4) the single pixel occupancy, defined as the probability of a single pixel to be over a certain threshold, plotted as a function of the threshold level normalized to the single pixel noise. To reach a $3x10^{-5}$ occupancy (i.e. less than one pixel per frame) a threshold of 5.5 times the pixel noise is enough. This would translate into an absolute cut of about 13 ADC counts to select events without contamination when an external source is activated.

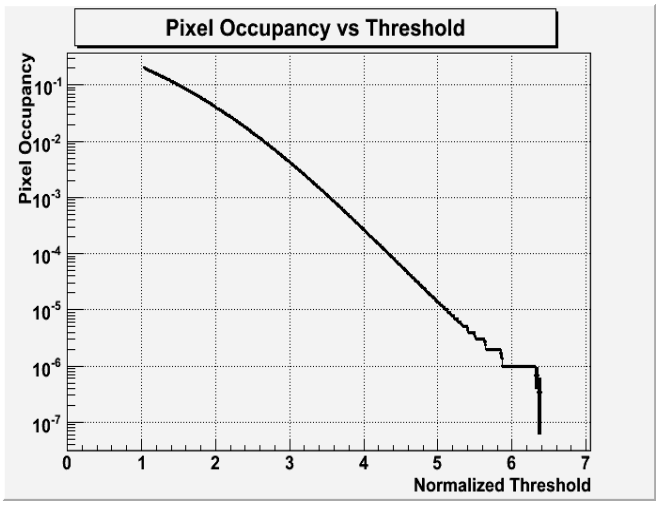

Fig. 4. Single pixel occupancy vs the normalized pixel threshold. At a threshold of 6.5 the pixel occupancy is less than one in ten billions. [7]

III. Characterization with Radioactive Sources

The characterization has been carried out using ionizing radiation sources (^{55}Fe, monochomatic X-ray sources, 500 MeV electron beam). In fig. 5 the sensor response to an X-ray photon has been reported. As can be seen just few pixels around the one with the maximum charge are interested by the signal. This implies a very good spatial localization of the signal, already observed when other CMOS pixel sensors developed by our group have been tested [1].

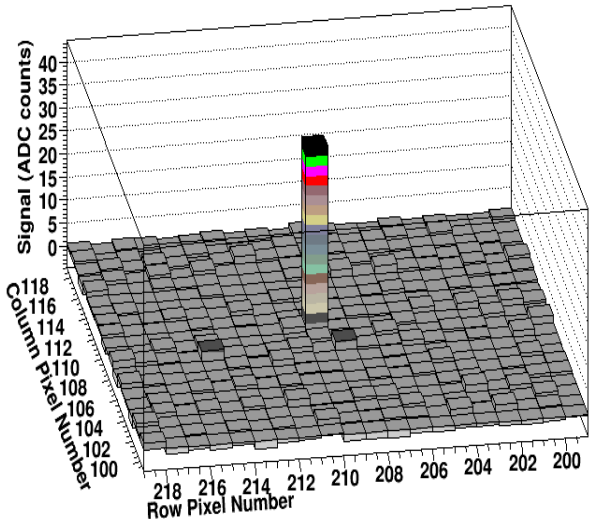

Fig. 5. Event display for an X-ray event ; few pixels are interested by the energy deposition .

It is necessary to define a procedure to sum up all the contributions from different pixels in order to recover as much as possible of the released charge. It is customary to use the sum of all the pixels of a submatrix centered around the seed pixel, defined as the pixel with a signal bigger than a certain threshold. Depending on the size of the matrix the signal is characterized by a cluster size of 3x3, 5x5, and so on. This approach has the disadvantage that while summing up all the possible contributions, also the pixel noise due to a growing number of pixels is summed up leading to an increase of the width of the signal distribution.

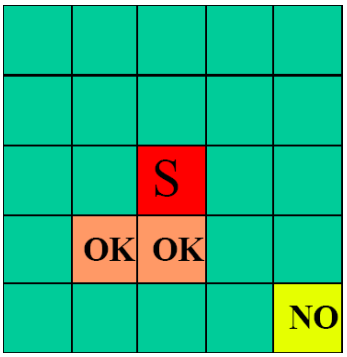

Fig. 6. Example of the application of the clustering algorithm: seed pixel with signal over V_{seed} (S); pixels with signal over V_{adja} and belonging to the cluster (OK); pixel with signal over V_{adja} and not belonging to the cluster because topologically disconnected (NO).

We have hence introduced an algorithm to define a *cluster*: in order to collect as much charge as possible whire reducing the introduction of pixel noise in the signal. First a seed pixel (S) is defined if its signal value is bigger than a seed threshold value (V_{seed}) normalized to the noise of the pixel (6.5 for these detectors); then all the pixels in the 3x3 matrix centered on the seed are tested to see if their signal is bigger than the adjacent

threshold value (V_{adja}) normalized to the pixel noise (3.0 for these detectors), in which case the pixel is added to the cluster; the procedure is repeated for the outer ring of the 5x5 matrix to select pixels with signal over V_{adja} and topologically connected to the cluster (fig. 6).

IV. Absolute Calibration for Cluster Signal

Fig. 7 shows the distribution of the number of pixels belonging to a cluster when a ^{55}Fe source is used with the V_{adja} = 3.0.

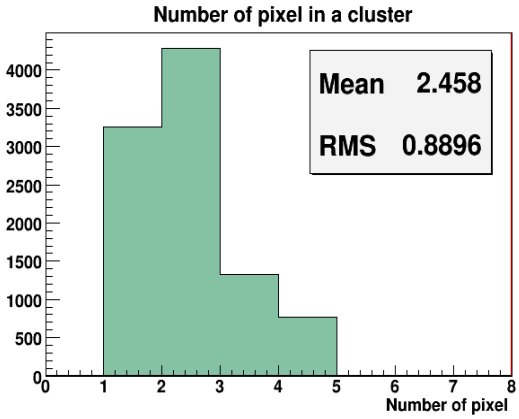

Fig. 7. Distribution of the number of pixels belonging to a cluster for X-ray photons.

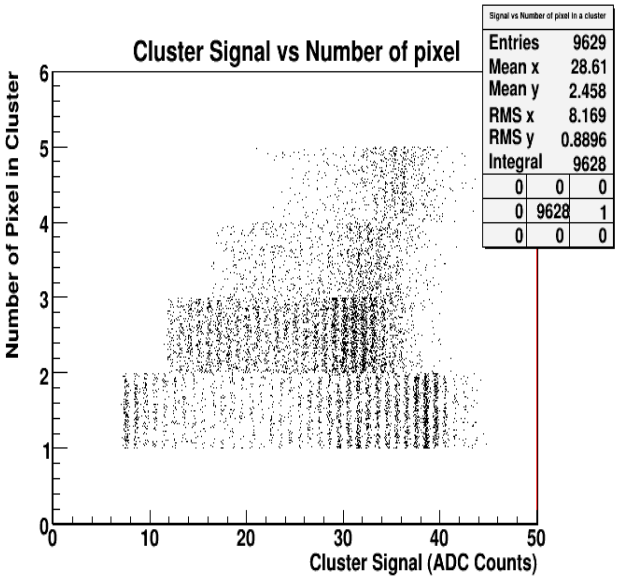

Fig. 8. Distribution of the cluster signal as a function of the number of pixels belonging to the cluster for X-ray photons. It is evident the charge collection loss when passing from one to more-than-one pixel clusters.

The average number is 2.8 peaked at 2 and no cluster has more than 4 pixels; this implies a good geometrical confinement of the signal in an area of few pixels, i.e. an area of the order of less than one hundred μm^2.Plotting the cluster signal (fig. 8) a charge collection loss for multi-pixel clusters has been found.

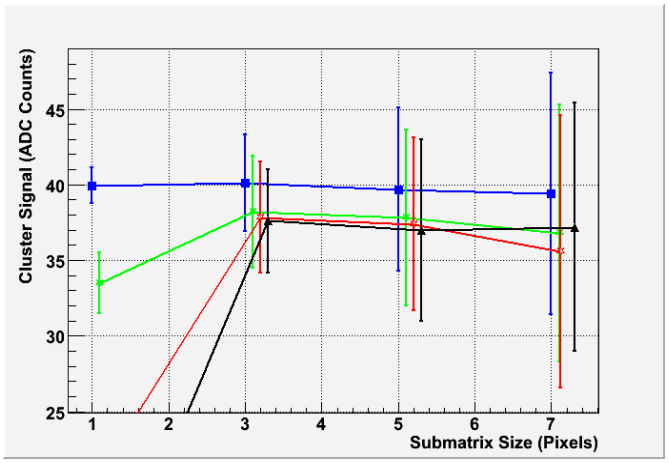

Fig. 9. Variation of the cluster signal with respect to the size of the submatrix to be considered. Blue line is for 1-pixel clusters; green line for 2-pixel clusters; red line for 3-pixel clusters; black line for 4-pixel clusters. It is clear the different behaviour between 1-pixel clusters and the other cluster categories.

This is not an artefact of the clustering algorithm because if we select the cluster with just one pixel over the V_{adja} threshold, and then compute the sum of the 3x3, 5x5 and 7x7 submatrices, we find for the signal a substantial invariance (~ 40) while if we select the other categories (2-, 3- or 4-pixel cluster) we find again a substantial invariance of the signal (~ 37-38) across all categories and all submatrices dimensions (fig. 9), with a difference of about 5-7%.

Another cross-check is presented in fig. 10 where for each category (1-, 2-, 3-, 4-pixel) the cluster signal has been computed varying the V_{adja} threshold. Again the difference between the 1-pixel case and the others could be seen irrespective of the V_{adja} threshold. Hence, in order to derive the absolute calibration for the detector only the 1-pixel clusters have been considered. Operating the sensor at unitary gain the double peak of ^{55}Fe can be observed (fig. 11) with an energy resolution of the order of 2-2.5%. The tail on the left side of the distribution is attributed to events where an incomplete charge collection took place, due mainly to the conversion depth of the photon.

A monochromatic 8 keV X-ray tube was also used to have another point in energy to derive the calibration line (fig. 12). Then a conversion factor of 34 ± 4 electrons/ADC count could be derived, from which an equivalent pixel noise of 8.5 ± 1.0 electrons is established.

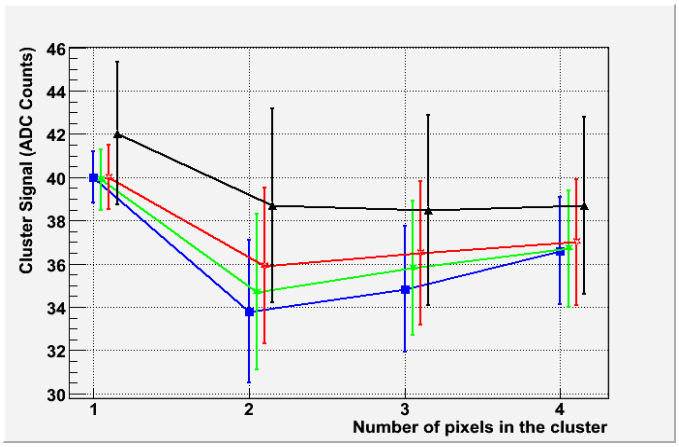

Fig. 10. Variation of the cluster signal with respect to the threshold Vadja. Blue line is for Vadja = 3.0 ; green line for Vadja = 2.5; red line for Vadja = 2.0; black line for Vadja = 1.5. For all curves the cluster signal drops when the number of pixels with a normalized signal bigger than 3.0 is two or more.

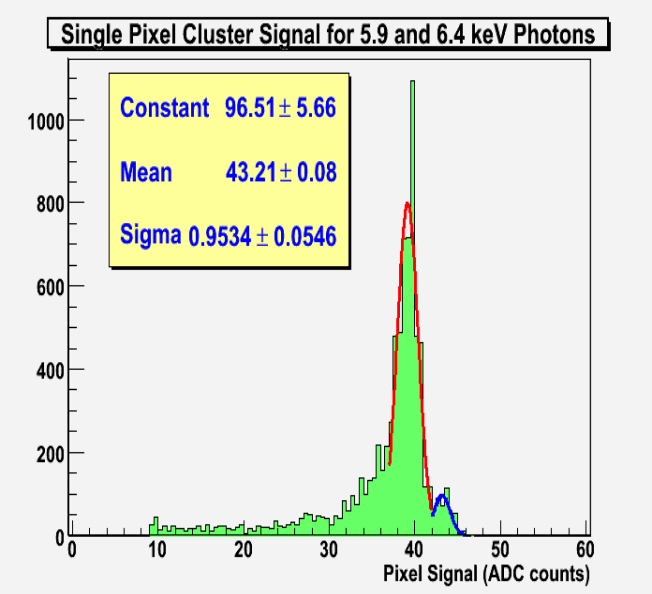

Fig. 11. Distribution of signal for 1-pixel clusters for 55-Fe photons; the double peak corresponding to the 5.9 and 6.4 keV could be clearly observed.

If the sensor is operated at maximum gain (G=15.88) then again a linear fit holds and from that a pixel noise of 9.7 ± 1 electrons, in good agreement with the low gain value, could be derived.

V. Characterization with 500 MeV electrons beam

Two detectors were put on the 500 MeV electron beam at the INFN Laboratori Nazionali di Frascati Beam Test Facility. They were setup face-to-face, and the DAQ was organized such a way that they were synchronously read-out and the event was recorded if one of the two has a pixel over a certain threshold, to allow an unbiased selection of events in the other sensor. In order to select a clean sample of events a simple geometrical correlation for X and Y coordinates has been used.

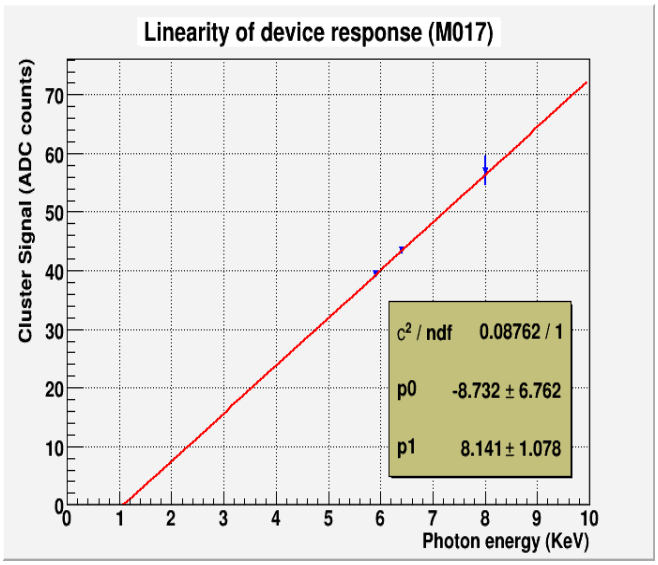

Fig. 12. Calibration line for Micron sensor obtained in unitary gain condition; a good linearity has been observed

The single pixel signal of the untriggered sensor (fig. 13) shows the expected shape with a pixel noise similar to the one found in laboratory tests and a tail toward high signals due to the pixels who collect part of the charge generated by the passage of the ionizing particle.

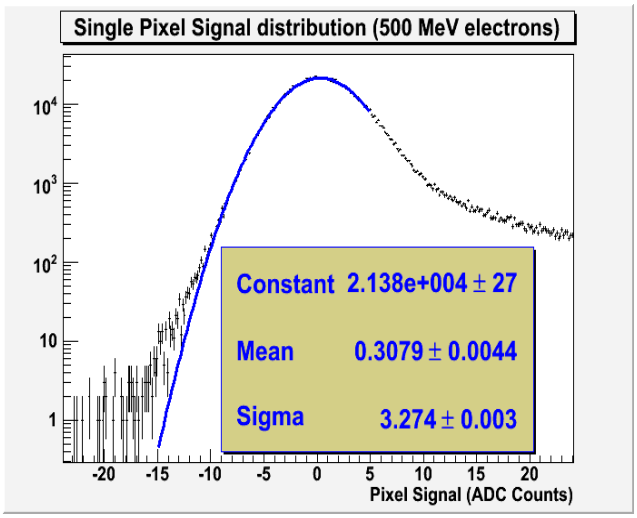

Fig. 13. Single pixel signal distribution for 500 MeV electrons at maximum gain (G = 15.88); the sigma of the gaussian peak centered at zero is an estimate of the average pixel noise. The right tail contains pixel who have collected signal due to the passage of the charged particle.

First for each cluster its X and Y coordinates have been found using the simple linear combination of the charge deposited in the pixels (baricenter). Using then the cluster position in the triggered sensor plane, all the couplings with the clusters found in the other sensor have been plotted for both coordinates defining the geometrical offset between the two sensors. Correcting for this effect the distribution of the pixel coordinates difference has been plotted (fig. 14) showing a peak around zero that corresponds to events where an electron has passed the triggered detector and then also the second

sensor following a straight trajectory. The width of the peak together with the distance between the two sensors gives a value for the beam angular spread of the order of 15-20 mrad that is what is expected from the beam parameters. Hence a fiducial geometrical region in the untriggered sensor could be defined to study an unbiased set of clusters.

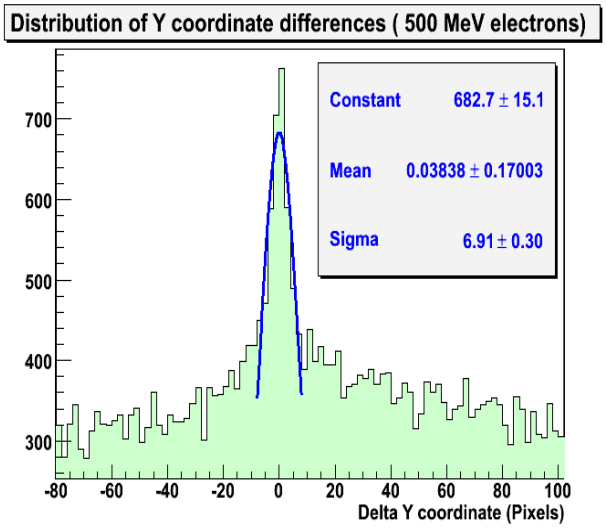

Fig. 14. Difference if Y coordinate for the clusters in the two sensors after offset correction. The narrow peak correspond to an electron beam with and angular divergence of 15-20 mrad, near to the beam parameters predictions.

In fig. 15 the distribution of the number of pixel in the cluster is shown. The distribution has an average value bigger than the X-ray one mainly due to the fact that the electron-hole creation takes place in a different volume of the detector in this case (a cylinder) with respect to the other (a rough sphere). The average value is 4.8 pixels, again compatible with a good geometrical confinement of the signal.

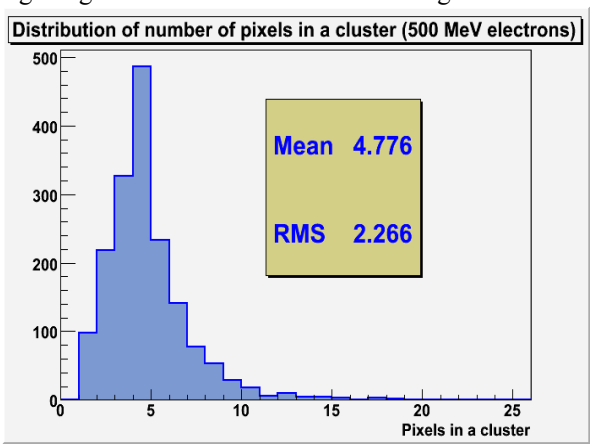

Fig. 15. Distribution of the number of the pixels in a cluster (500 MeV electrons).

In fig. 16 the cluster signal distribution is shown for both triggered than untriggered events. The two distributions show almost no difference in both shape than MPV and width. Hence we could use one set of events or the other without incurring in any relevant error due to the biased sample collected using the autotriggering scheme .Using the absolute calibration a value of ~ 300 ± 13 electrons is found for the MPV of the distribution, corresponding to a S/N ~35 ±4.

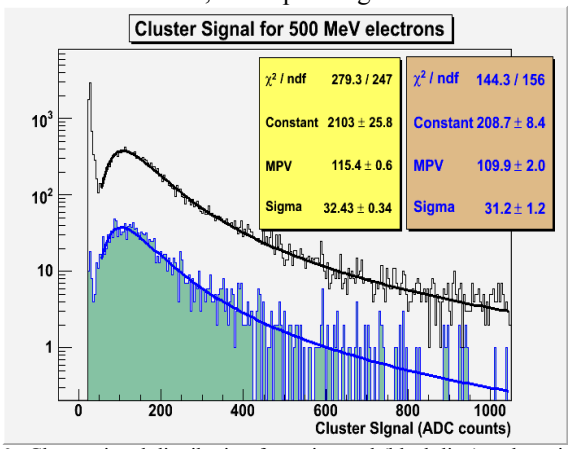

Fig. 16. Cluster signal distribution fron triggered (black line) and untriggered (blue line) events with Landau fits superimposed. The difference of the two distribution is almost negligible, few % of the MPV.

Using the typical value of 95 created pairs/micrometer for 500 MeV electrons , an estimation of 29 ± 4 for the S/N of a Minimum Ionizing Particle (MIP) could be derived Also the equivalent thickness of the signal collection region could be estimated in 3.15 ± 0.4 micrometer, in reasonable agreement with the 4 micron depth of the epitaxial layer.

VI. Conclusions

A standard CMOS imager has been tested both electrically than with ionizing radiation sources to assess its suitability as ionizing radiation detector. First of all a good response linearity as been measured in all the device gain range. A good geometrical confinement of the signal has been found (just few pixel in the immediate neighborhood of the seed pixel) either for X-ray photons than for charged particles, thus allowing in principle a very good spatial resolution. A Signal/Noise value of 29 ± 4 has been derived for MIPs, far from the threshold value of 6.5 needed to avoid fake hits with a rate of less than one part in 10 billions. We conclude that the sensor could be suitable to be used as ionizing radiation detector, depending on the applications and that further work is needed to measure efficiency, spatial resolutions and resistance to radiation damage.

Acknowledgment

The authors gratefully acknowledge dr. Andrea Del Monte and dr. Alfonso D'Anna (Micron Technology Italia) for their fruitful discussions and contribution, and prof. F. Sacchetti (University of Perugia) for the use of his X-ray laboratory instrumentation.

References

[1] L. Servoli, et al. " Test of a MAPS realized in standard non-epitaxial CMOS 0.18 μm technology ", *Nucl. Instr. Meth.A581 335-338 (2007).*